Weather and Climate Extremes 41 (2023) 100588

Contents lists available at ScienceDirect

Weather and Climate Extremes

journal homepage: www.elsevier.com/locate/wace

Evolution of heatwaves in Chile since 1980

Álvaro González-Reyes [a,b,c,d,e,*], Martín Jacques-Coper [f,h,j], Claudio Bravo [g], Maisa Rojas [h,i], René Garreaud [h,i]

[a] Instituto de Ciencias de la Tierra, Facultad de Ciencias, Universidad Austral de Chile, Valdivia, Chile
[b] Hémera Centro de Observación de la Tierra, Universidad Mayor, Chile
[c] Centro de Humedales río Cruces CEHUM, Universidad Austral de Chile, Chile
[d] Laboratorio de Dendrocronología y Cambio Global, Universidad Austral de Chile, Valdivia, Chile
[e] Centro de Investigación: Dinámica de Ecosistemas Marinos de Altas Latitudes - IDEAL, Chile
[f] Departamento de Geofísica, Universidad de Concepción, Concepción, Chile
[g] Centro de Estudios Cientificos CECs, Valdivia, Chile
[h] Center for Climate and Resilience Research (CR)2, Chile
[i] Departamento de Geofísica, Universidad de Chile, Santiago, Chile
[j] Center for Oceanographic Research COPAS-COASTAL, Universidad de Concepción, Concepción, Chile

ARTICLE INFO

Keywords:
Heatwaves
Megadrought
Extreme weather events
Puelche winds
Chile

ABSTRACT

Heatwaves (HWs) are highly dangerous threats to human and ecosystem health, as well as to many economic sectors around the world. In the present work focused on Chile, we use a high-resolution (~5 km) gridded product (CR2Met v2.0) to evaluate the spatiotemporal distribution and trends of HWs. We analyze daily maximum temperatures (Tx) from late austral spring to early autumn (November to March) to evaluate the HWs behavior during 1980–2020, using three criteria: i) three consecutive days with Tx > 30°C, ii) three consecutive days with Tx > 90th percentile (P90), and iii) three consecutive days with Tx > 95th percentile (P95). We validated our results using HWs statistics based on eighteen official meteorological stations; this procedure revealed a coherence with gridded data mainly over the Central Valley and the Andes. Using the P90 threshold, we found upward trends across the Andes between 20° and 36°S (>1 events per decade), and in the Central Valley between 34° - 43°S (>0.75 events per decade). In addition, using the P90 and P95 thresholds, HWs exhibit upward trends (>1 and 0.5 events per decade, respectively) throughout most of Chile, including Andes and Patagonia. Moreover, using all thresholds, we found an increase in HW frequency during the 2011–2020 megadrought period (ranging from 1 to 4 HWs events/decade) in comparison to the previous period (1980–2010). Meteorological factors such as an increase in the frequency of Puelche (Föhn-like) winds are proposed as an amplifying mechanism of HWs in South-Central Chile.

1. Introduction

Climate extreme events such as heatwaves (HWs), defined as a sequence of consecutive days with warmer than normal conditions for a particular region and period of the year (Perkins 2015), have been shown to be a devastating event around the globe, with severe consequences to the health of people (e.g., cardiovascular and dehydration problems; McMichael and Lindgren 2011) and the environment (e.g. wildfires rapid propagation; Bowman et al., 2017, De la Barrera et al., 2018). Prolonged periods of high temperatures impact economic sectors (Kjellstrom 2016) including substantial problems and losses in the agriculture sector (Thornton et al., 2009). On a global scale and according to the World Health Organization (WHO), between 2000 and 2016 the number of people exposed to HWs increased by around 125 million. Following the recent report of the (Intergovermental Panel on Climate Change, 2021), a consensus exists about an increase of the intensity and duration of heatwaves in most regions of the world since 1950. In continental Chile, lying between the Pacific Ocean and the Andes Cordillera from 17°S to 56°S, recent HWs have provoked substantial ecosystem losses. For instance, during January 2017, daily maximum air temperature continuously reached values above 30°C between 30° to 40°S, and ~5 000 km^2 of native forest and exotic plantations were burned during the so-called "firestorm" (Bowman et al., 2019). The burned area during 2017, was ten times the average

* Corresponding author. Instituto de Ciencias de la Tierra, Facultad de Ciencias, Universidad Austral de Chile, Valdivia, Chile.
E-mail address: alvaro.gonzalez@uach.cl (Á. González-Reyes).

https://doi.org/10.1016/j.wace.2023.100588
Received 29 October 2022; Received in revised form 30 May 2023; Accepted 19 June 2023
Available online 20 June 2023

area burned in the previous 40 years as has been reported by Urrutia--Jalabert et al. (2018). Despite Chile's environmental consequences during the "firestorm" in 2017, the study on HWs in Chile has received small attention to date. On the other hand, most of Chile has experienced a persistent dry period (called "mega-drought", hereafter MD) since 2010, without replicates within a millennial context (Garreaud et al., 2017). This extreme dry interval is framed within a severe long-term rainfall reduction recorder along Chile (Quintana and Aceituno, 2012; González-Reyes 2016; Boisier et al., 2018). The HWs frequency during the MD has not been quantified to date.

The climate variability in Chile is, to a large extent, related to tropical forcing as El Niño Southern Oscillation (ENSO) on interannual scales, being a key driver of precipitation variability in northern-central Chile (18°-35°S; Rutlant and Fuenzalida, 1991). High latitudes climatic forcing such as the Southern Annular Mode (SAM), which controls the north-south migration of the southern westerly wind, modulate rainfall and temperature variability in Chile, particularly over southern Chile (Garreaud et al., 2009; Holz et al., 2017). In addition, a recent study indicates that HWs in Central Chile can be partially forced by intra-seasonal precursors stemming from the extra-tropics, such as the South Indian Ocean, and the tropics, via the Madden-Julian Oscillation (MJO), so they tend to occur during active MJO phases 6 and 8 (Jacques-Coper et al., 2021).

Several works have been carried out to evaluate HW trends in larger areas, including Chile (Donat et al., 2013; Ceccherini et al., 2016). However, only the study by Piticar (2018) performed a systematic analysis of HW trends in Chile during 1961–2016 using station data. Using multiple HWs definitions based on the World Meteorological Organization (WMO), Piticar (2018) analyzed temperature (maximum temperature: Tx, minimum temperature: Tn) records from twelve official meteorological stations managed by Dirección Meteorológica de Chile (DMC), focusing on their intensity, duration, and frequency. The study found increasing trends in most analyzed HW indices. In particular, the number of HW events based on Tx showed the highest amount of upward trends along Chile. Spatially, Piticar (2018) found more pronounced changes in central Chile; for instance, considering again HW number based on Tx for Santiago (the capital city), the reported trend was 0.30 events/decade. The results from Piticar (2018) are highly relevant but restricted to a dozen of stations in the full county that extends more than 4 000 km in the meridional direction and includes sharp topographic gradients, thus calling for further analyses. Feron et al. (2019) combined observations and global circulation models to assess past and future HW metrics over South America and selected major cities, finding greater increases in HW in the northern than the southern part of the continent by the mid-21st century under the RCP8.5 scenario. Moreover, recent studies have focused on mechanisms leading to HWs mainly in central and Southern Chile, including synoptic patterns and precursors (Jacques-Coper et al., 2021; Demortier et al., 2021). However, there is a gap concerning the spatiotemporal assessment of HWs: using high-resolution gridded products across Chile allows the identification of regional patterns that are not evident when analyzing records from single stations. This is particularly true in Chile, where the station network is sparse and few long-term records are available. Specifically, regional patterns of climate change are relevant for climate change impact assessment, especially over a complex topography as is the case of Chile's. In a similar way, regional patterns of HW trends are crucial for the risk assessment of compound extreme events. This perspective is highly useful and necessary taking into consideration: i) the current dry interval experimented in Chile since 2010 (known as the Megadrought, MD) and water crisis evidenced in several valleys of Central Chile (Muñoz et al., 2020), ii) the number and magnitude of recent forest fires, especially those occurred during 2017 and 2023, and iii) the agricultural vocation of the country, economic activity that exhibits high vulnerability to climate change (Ponce et al., 2014).

Another impact linked with the increasing trend in HWs is related to the mass loss of glaciers as well as their contribution to runoff. HWs lead to rapid snow cover loss, notably if these events occur early in the ablation season (e.g., October to November in Chile), exposing a large portion of bare ice for a more extended period (Pelto et al., 2022). In consequence, glacier melting along the ablation season is enhanced, and the ice mass loss increases. Furthermore, although not evaluated yet in the Andes, the increased number and frequency of HWs are impacting the glacier contribution to baseflow during summer months as well as the temperature of the meltwater as seen elsewhere (e.g., Pelto et al., 2022). The changes in the Andean glaciers melt dynamics and timing due to HWs will probably impact water resources availability at medium to large term in rivers highly dependent on glacier meltwater, especially the runoff at the end of summer (Bravo et al., 2017; Ayala et al., 2020).

Given this background, the aim is to study HWs along Chile based on a high-resolution, country-scale gridded product and detect potential hotspots. The specific goals of this study are: i) to examine HW trends during 1980–2020 based on station data and the CR2Met gridded product, ii) to evaluate (and, if possible, validate) HW trends obtained from the gridded product using in situ meteorological measurements, iii) to compare HWs statistics during 1980–2010 and 2011–2020 (the megadrought period), iv) to explore potential mechanisms driving conspicuous HW trends. The paper is organized as follows: Section 2 describes the data and methodologies. The results are presented in section 3 and the discussion is presented in section 4, where we also included several environmental impacts of HWs along Chile. Finally, section 5 contains the main conclusions of this research.

2. Data and methodology

Our study area corresponds to the whole Chilean continental territory (17° - 56°S) encompassing a diversity of climate types. Sarricolea et al. (2017) group the climate types in continental Chile as arid (according to Köppen classification: desert climates BWh and BWk, along with semi-arid climate BSk), temperate (including Mediterranean climates Csb, Csc, and marine climates Cfb, Cfc), and polar (including tundra climates ET, and ice cap climates EF). Correspondingly, the summer mean (November to March 1981–2010) minimum (Tn), mean (Tas), and maximum (Tx) temperatures present a heterogeneous spatial distribution along Chile as inferred from CR2Met v2.0 (CR2Met onwards; Fig. 1 and Fig. S1). CR2Met is a high-resolution gridded product, with ~5 km horizontal resolution, that was developed within the Center of Climate and Resilience Research (CR)2 by integrating station data, ERA5 reanalysis data (Hersbach et al., 2020), and MODIS satellite observations (Boisier 2023). This product, which spans from January 1979 to March 2020 at daily resolution, is available at http://www.cr2.cl/datos-productos-grillados/, and has been used in previous studies (Alvarez-Garreton et al., 2018; Bozkurt et al., 2019, Martínez-Retureta et al., 2021; Aguirre et al., 2021). For the assessment of circulation patterns associated with salient trends in HWs over selected regions, we focus our analysis on possible relationships with Puelche (Föhn-like) winds. For this, we use the daily zonal wind at 850 hPa (U850) from the ERA5 reanalysis (Hersbach et al., 2020) regridded at ~ 5 km using a bilinear interpolation. We computed daily U850 averages for NDJFM 1980–2020 considering gridded values at 00, 06, 12, and 18 UTC. Puelche events (i.e., easterly flow) over a certain area are those days whose corresponding spatially averaged daily U850 values are equal or below -4 m s^{-1}, following the threshold given by Montecinos et al. (2017). Finally, for selected regions, we compared the seasonal frequency and intensity of Puelche events with the frequency of HWs based on the three definitions.

To analyze HWs, we considered daily Tx from CR2Met from November to March (NDJFM) and the year corresponds to that of JFM. Our analyzed period spans from November 1980 to March 2020. To identify HWs, we used three criteria, namely that Tx surpasses for three consecutive days the thresholds of i) 30 °C (30C), ii) its NDJFM 90th percentile (P90), and its NDJFM 95th percentile (P95). The 30°C value was chosen because it is commonly considered ("rule of thumb") as a

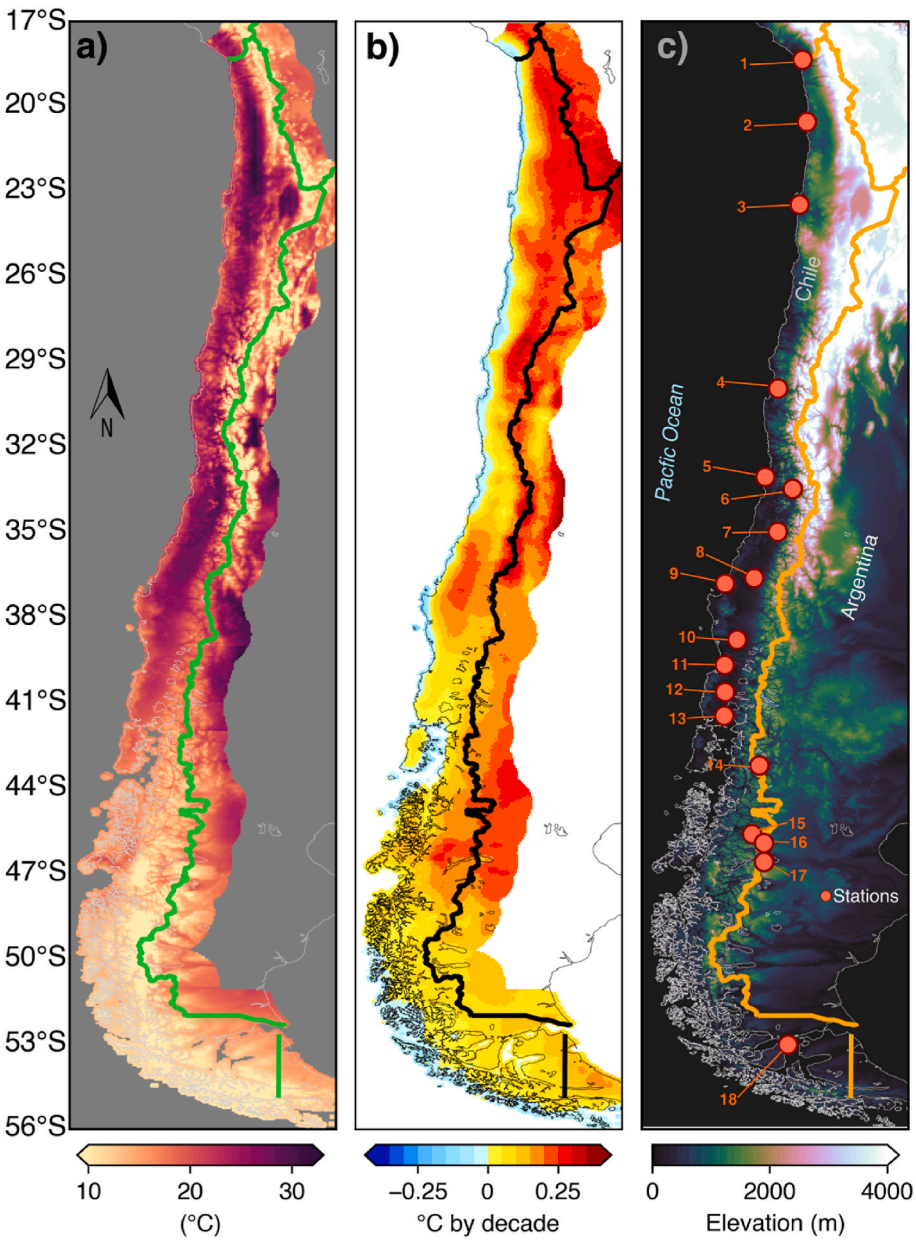

Fig. 1. November–March climatology of maximum temperature (Tx) based on CR2Met for 1981–2010. b) November–March Tx trends evaluated during 1980–2020. Changes in Tx are expressed in °C by decade. c) Location of each meteorological station (Table 1) and elevation (in meters) based on the Shuttle Radar Topography Mission SRTM-DEM at 90 × 90 m product.

temperature threshold above which rapid propagation of wildfires may occur; additionally, it is a subjective value based on the social perception of extreme heat in Chile. The P90 and P95 percentiles were calculated for NDJFM 1981–2010 on a seasonal basis (Fig. 2). Then, we counted the total number of HWs detected during each season. Additionally, we validated CR2Met Tx for 1980–2020 using records from 18 meteorological stations operated by DMC (Table 1 and Fig. 1c) and the neatest gridpoint, based on three statistical metrics: R-squared (R^2), Root Mean Square Error RMSE, and Bias (expressed in °C). A detailed description of the DMC Tx data can be found in Piticar (2018). The statistical metrics described before were computed using the "metrics" package (free available in: https://github.com/mfrasco/Metrics) to the free R-project software (R Core Team 2020). We calculate temperature and HW frequency trends using least-squares linear regression; and express their slope "m" in °C per decade and events per decade, respectively. We also contrast HW trends using CR2Met and observed Tx.

3. Results

3.1. Temperature climatology

We first describe the 1981–2010 NDJFM temperature climatology for Chile based on CR2Met. The distribution of maximum temperatures is affected by both latitude, altitude, and closeness to the ocean (Fig. 1a). Tx (Fig. 1a) shows high values (~17° to above 30°C) along coastal locations between ~ 20° to 26°S, around 30°S, and between ~32°-42°S. On Andes locations along these latitudes, Tx exhibits values between 5° to 15 °C. Southward of 42°S, Tx shows values between 0° to 15°C. A key point for this study is that Tx over 30°C is observed in Northern Chile within 20°–25°S and the Central Valley, an elongated depression between a coastal range and the Andes extending from 34° to 37°S.

Before identifying HWs, we computed the main statistical thresholds (R^2, RMSE, and Bias) based on Tx from observations and CR2Met, for NDJFM 1980–2020 (Figs. S2a–d). Concerning R^2 (Fig. S2a), we

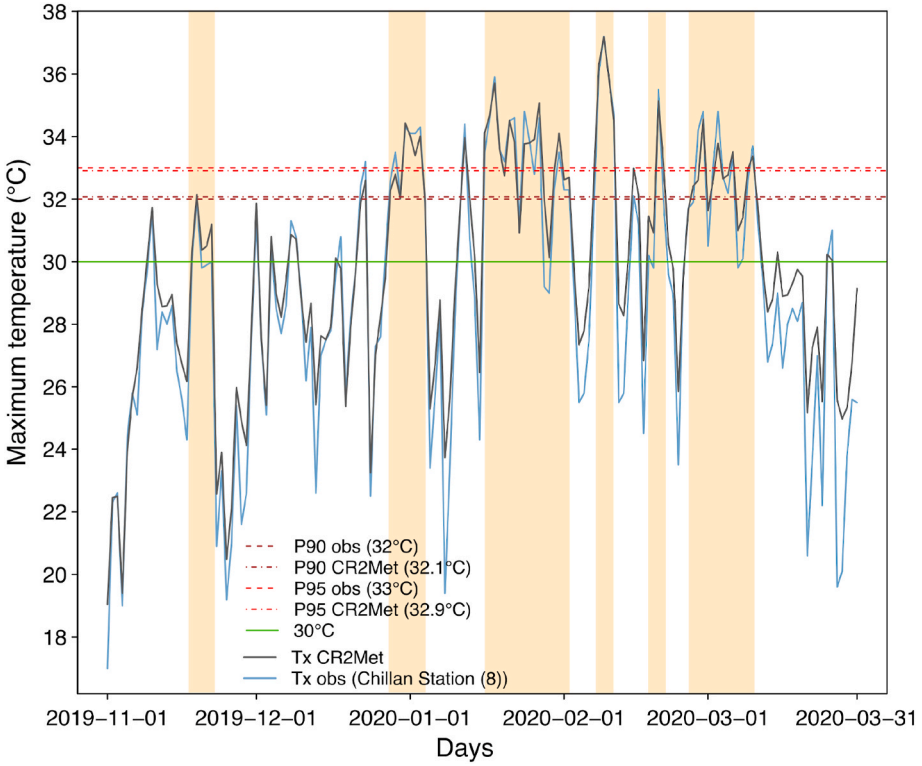

Fig. 2. Comparison between daily maximum temperatures recorded at Chillan station (number 8 in Table 1, light blue) and the closest CR2Met gridpoint (black) during November 2019 to March 2020 (i.e., NDJFM, 2020). Horizontal dashed and continuous lines indicate the thresholds used to compute heatwaves: 90th percentile P90, 95th percentile P95), and 30°C (30C), all computed for 1981–2010. Vertical bars indicate heatwave episodes. (For interpretation of the references to color in this figure legend, the reader is referred to the Web version of this article.)

identified low (around 0.30) values mainly at coastal stations along the North (station 1 ARI and 2 IQU) and in Central Chile (station 6 STG), while R^2 values (Fig. S2a) are higher (between 0.4 and 0.45) in stations to the south of 37°S (station 9 CON). In the case of RMSE (Fig. S2b), we observe values mostly between 1.5 and 2, with the lowest value at station number 1 (ARI) and the highest value at station number 4 (LSE). The bias between both sources of daily Tx records (Fig. S2c) exhibits mostly negative (i.e., an overestimation of CR2Met) values between -3° to −1°C, while positive values (i.e., an underestimation of CR2Met) are observed at station 2 (IQU), and from station 14 (FUT), station 15 (COY) and on station 17 (CCH), with values between 1° and above to 2°C.

3.2. Heat waves: frequency and trends

HW frequency seems to be satisfactorily reproduced by CR2Met (Fig. S2). This might arise from the fact that HW is, per definition, an extreme event that combines intensity and persistence. These aspects seem to be captured by CR2Met. As a reference, we compare in Fig. 2 the observed and the CR2Met Tx and their corresponding thresholds (P90, P95, and 30C) during NDJFM 2019–2020 for station 8 (CHI), located at 36°S within the Central Valley (Table 1, Fig. 1c). Beyond the validation metrics, HWs events are well captured by CR2Met. To emphasize this conclusion, we validated NDJFM HW frequency trends derived from observed and CR2Met Tx at the 18 DMC stations (Fig. S3a-r).

Tx shows mostly upward trends across Chile during 1980–2020 (Fig. 1b). The trends are larger between ~20° and 30°S (from 0.2° to 0.4°C per decade), between 35°-40°S, and ~45°-50°S (0.3°C per decade). Most of Patagonia exhibits an upward trend of 0.1°C per decade. Nonetheless, downward Tx trends were identified along the coast of North Chile (around −0.1°C per decade). This is comparable with −0.2°C per decade reported for Tas during 1979–2006 by Falvey and Garreaud (2009) due to the intensification of the South Pacific Anticyclone. Overall, the trends in Tn and Tas are similar to their Tx counterparts, with a dominance of upward trends except for the coast of northern Chile (Figs. S1c–d and Fig. 1b, respectively).

Concerning the validation of the HW frequency trend, there is a general agreement between both data sources. Trends based on the 30C threshold (Fig. S2d) exhibit upward patterns from station 6 (STG) to 8 (CHI), and at 10 (TEM). Higher HW frequency trends are found for observations than CR2Met, particularly at stations 6 (STG) and 7 (CUR), with values ranging between 2 and 2.5 events per decade on these stations. A similar trend was identified at station 8 (CHI). However, a higher trend of 0.3 events per decade was found at station number 10 (TEM) based on CR2Met. Using the P90 threshold (Fig. S2e), a clear upward HW frequency trend was found in stations 6 to 8 and 10 to 17 based on both products. Conversely, while downward HW frequency trends were identified at stations 1 to 4 based on observations, CR2Met does not show this clearly. Stations 1 (ARI) and 5 (VPO) exhibit inverse HW frequency trends based on CR2Met and observations. Slightly upward (downward) trends were found at stations 9 (CON) and 18 (PAR) based on observations (CR2Met). A similar pattern was registered based on the P95 threshold (Fig. S2f). Stations along the coast in the North exhibit downward trends based on observations, a result that is not reproduced by CR2Met. We identify downward observation-based HW frequency trends in stations number 1 (ARI) to 3 (ANT), and a slight downward trend in Central Chile on station number 9. On the contrary, CR2Met-based HW frequency trends at the same stations are lower, including opposite values at station 1 (ARI), as found for the P90 threshold. The highest observation-based HW frequency trends were identified at station 7 (CUR), with values around 1.5 (1) HW events per decade based on the P90 (P95) threshold.

The mean HW frequency based on the 30C threshold for NDJFM 1980–2020 shows two spatial clusters, located between ~20°-25°S and 33.5°S to 39°S, with values between 1 and 4 events per season (Fig. 3a). In addition, we identified some locations with similar values along the Central Valley, e.g., around 27°S and 30°S. HWs based on the P90 threshold (Fig. 3b) exhibit 3 events per season on average in Northern Chile (20°-24°S), and mostly along the Andes (~20°-35°S). The Central Valley (30°-42°S) exhibits between 1 and 2 events per season, North Patagonia (between 45° and 50°S), exhibits 2 and 3 events per season and Tierra del Fuego (55°S southward), between 1 and 2 events per season. The pattern observed using the P95 threshold is spatially

Table 1
List of the meteorological stations considered in this study and used to compute heat waves. The daily maximum temperature spanning the 1980–2020 of each station has been considered. Heatwaves have been calculated during November to March months. The missing percentage in all stations is 0.5% with respect to November to March, and calculated during the 1980–2020 period. All stations are addressed by Dirección Meteorológica de Chile DMC. Latitude and longitude are expressed in decimal coordinates and ordered from North to South.

Number	Code	Name	Elevation (m)	Longitude (°W)	Latitude (°S)
1	ARI	Chacalluta Arica Ap.	63	−70,3358	−18,3514
2	IQU	Diego Aracena Iquique Ap.	52	−70,1786	−20,5397
3	ANT	Cerro Moreno Antofagasta Ap.	113	−70,4411	−23,4503
4	LSE	La Florida La Serena Ad.	142	−71,2011	−29,9175
5	VPO	Punta Ángeles Valparaíso	330	−71,6475	−33,0278
6	STG	Quinta Normal Santiago	527	−70,6828	−33,445
7	CUR	General Freire Curico Ad.	225	−71,2167	−34,9664
8	CHI	Bernardo O'Higgins Chillán Ad.	151	−72,04	−36,5872
9	CON	Carriel Sur Concepción.	12	−73,0622	−36,7792
10	TEM	Maquehue Temuco Ad.	92	−72,6369	−38,77
11	VAL	Pichoy Valdivia Ad.	21	−73,0808	−39,6506
12	OSO	Canal Bajo Osorno Ad.	61	−73,0608	−40,605
13	PMT	El Tepual Puerto Montt Ap.	85	−73,0978	−41,435
14	FUT	Futaleufú Ad.	347	−71,8525	−43,1889
15	COY	Teniente Vidal Coyhaique Ad.	310	−72,1086	−45,5939
16	BAL	Balmaceda Ad.	517	−71,6942	−45,9128
17	CCH	Chile Chico Ad.	306	−71,6928	−46,5808
18	PTA	Punta Arenas	38	−70,845	−53,0033

homogeneous throughout Chile (Fig. 3c) showing 1 HW event per season. Some locations in Northern Chile, between 20° and 21°S in the Andes register 2 events per season. No events (as per P95) were recorded along coastal areas between ~30°-36°S.

HW frequencies across Chile based on the 30C threshold (Fig. 3d) exhibit an overall increase during 1980–2020, with upward trends in Northern Chile (~20°-25°S; 1.5 events per decade) and in Central and South-Central Chile (33.5°-39°S, between ~ 0.75 and 1.25 HWs events per decade). Upward trends are also identified in most of Chile based on the P90 threshold (Fig. 3e), particularly in the Andes (~20°-35°S) and along the Central Valley (~35°-37°S), with trends of 1 event per decade or stronger. Along the Central Valley (from 37° to 41°S), a trend of 0.5–1 HWs events per decade is observed, whereas in Patagonia (44° - 50°S) recorded values of 0.5–1 event per decade. The southern tip of Chile (50° southward) recorded between 0.25 and 0.5 events per decade. Conversely, slightly downward frequency trends were identified along the coast between 20° and 40°S and some locations in Tierra del Fuego. Finally, using the P95 threshold (Fig. 3f), upward trends were found in most of Chile, particularly along the Andes from the north (27°S) to central Chile (35°S). Values reach ~0.5 events per decade between 20° and 50°S. In addition, upward trends (~0.25 events per decade) were recorded in Tierra del Fuego, from 50°S southward. Conversely, coastal zones between 20° - ~40°S and the Tierra del Fuego exhibit slightly downward trends of ~ −0.25 events per decade.

3.3. The ongoing megadrought period (2011–2020)

In this subsection, we examine the mean NDJFM HW frequencies during the ongoing megadrought (2011–2020). Using the 30C threshold (Fig. 4a), the regions between ~20°-25°S and 33.5°S to 39°S recorded between 1 and 8 events per season on average (Fig. 4a). Using the P90 threshold (Fig. 4b), the region spanning from the north to Central Chile (~20°-35°S) recorded between 5 and 8 events per season, while the region located between 25° and 35°S, mostly on the Andes, recorded 6 events per season. In addition, the region spanning from ~35° to 43°S along the Central Valley exhibits between 3 and 5 events per season. Regions around ~35°S, and from 40° to 43°S (including the Chiloe Island) show clusters of high HW frequencies, with values around 5 events per season. While North Patagonia (45°-50°S) exhibits values between 3 and 5, South Patagonia (including Tierra del Fuego) shows from 1 to 3 events per season. Similar results for the P90 threshold were obtained using the P95 threshold (Fig. 4c). The Andes between 25° and 35°S exhibit values greater than 3 events per season, with some Andean valleys reaching a value of 4 events. The Central Valley (from 35°S southward) exhibits 2 and 3 events per season, just 1 is observed along the coast. Patagonia recorded a mean frequency of 1 event per season, whereas almost no HWs were determined in the coastal areas from 50°S southward. Concerning the differences in seasonal HW frequency between the megadrought period (2011–2020) and the previous decades (1980–2010), positive changes between +1 and + 5 events per season were recorded between~20°-25°S and 33.5°S to 39°S based on the 30C threshold (Fig. 4d). In the case of the P90 threshold (Fig. 4e), the region encompassed from the north to Central Chile (20°-35°S), particularly on Andes shows increases (between +2 and +4 events per season, particularly around 29°S and 34°S in the Andes, along with the Central Valley from 35° to 43°S, including the Chiloe island (between +1 and +3 HWs events per season). While Patagonia exhibits increases between +1 and + 2 events per season, no change is detected in Tierra del Fuego (from 50°S southward). A similar pattern is obtained using the P95 threshold (Fig. 4f): increases around 23°S and between 25° and 35°S in the Andes (+2 to +3 events per season), as well as around 35°S in the Central Valley (+1 to +3 events per season). Finally, the region spanning from 35°S southward shows a lower increase (+1 event per season). No changes were recorded in several coastal locations around ~30°S, 33°S, and 37°S.

3.4. Role of local climatic mechanisms

In Chile, synoptic patterns such as the intensity and the latitudinal position of the Southeastern Pacific Anticyclone (SPSA) during NDJFM are relevant to understand the variability in HW frequency. Ancapichún and Garces-Vargas (2015) found an intensification and southwestward shift of the SPSA during 2000–2012. Furthermore, transient (migratory) anticyclones also exhibit a trend toward a southward-shifted track (Aguirre et al., 2019). These migratory anticyclones induce, in turn, Foehn-like downslope easterly flow that led to clear skies and hot and dry conditions along 35°-41°S (Montecinos et al., 2017). We speculate that both factors could be the main controllers of HWs frequency and intensity in South-Central Chile and Patagonia. To expand on this, we defined a region between 38° and 40°S and used Tx from CR2Met and U850 from ERA5 to explore a possible relationship between Puelche winds and HWs. For this, we set a threshold of U850 < -4 m s^{-1} to define Puelche events. We found positive and significant correlations between P95 HWs and Puelche frequency in this region (Fig. 5a). Based on these results, we selected two subdomains (denoted s1 and s2) in order to focus on atmospheric processes occurring within the mesoscale (i.e., a few hundred kilometers). The relationship between the average Tx CR2Met and U850 ERA5 within subdomain s1 shows a nearly linear increase in Tx due to an increase in the intensity of easterly wind during Puelche events (Fig. 5b). In addition, a positive and significant relationship between the annual mean frequency of Puelche events and P95

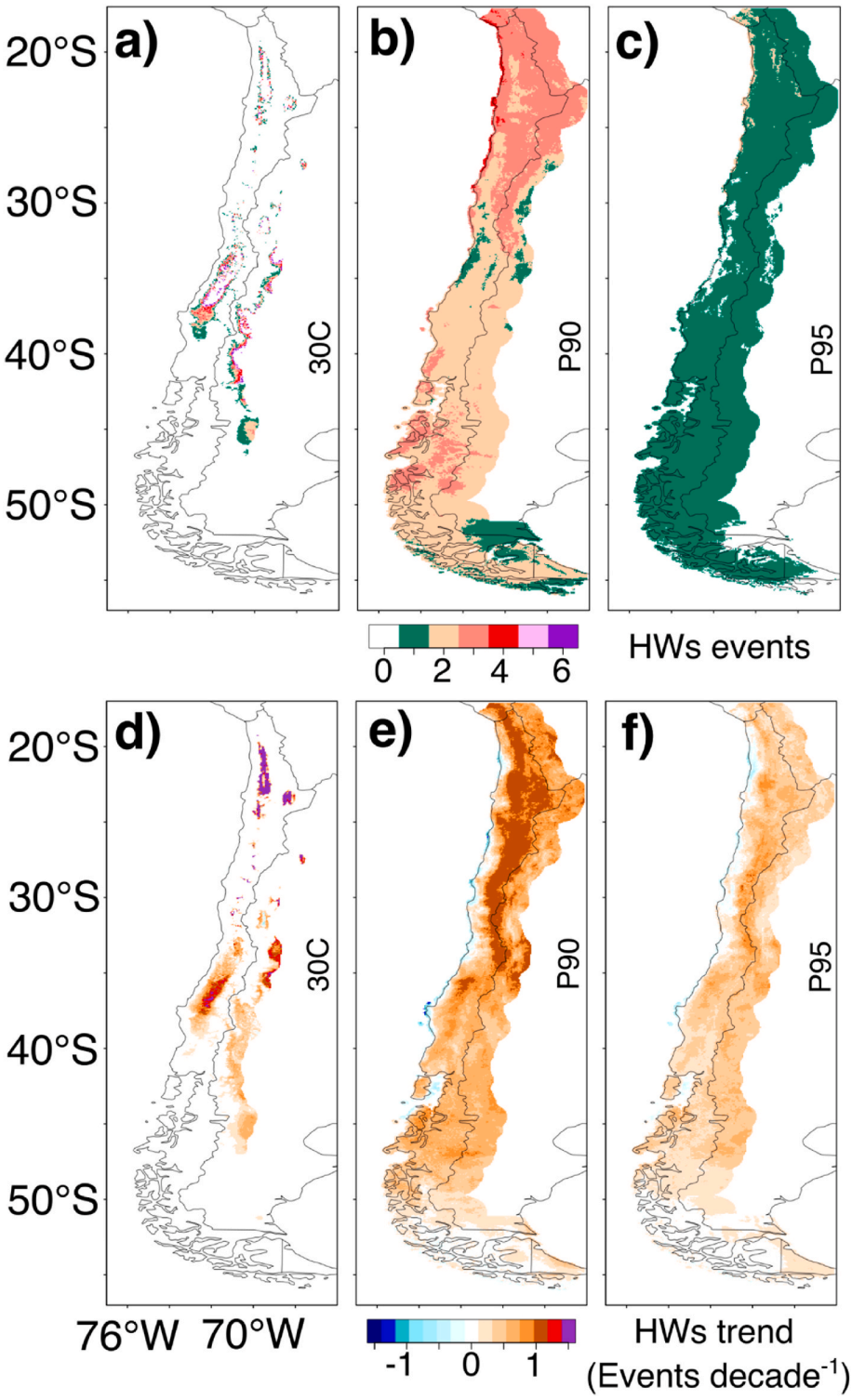

Fig. 3. a-c) Mean heatwave frequency for 1980–2020 based on the 30C, P90, and P95 thresholds, respectively. d-f) Similar to a-c, but for heatwave frequency trends expressed in events per decade.

HWs is recorded on the s1 subdomain during 1980–2020, after removing the first-order autocorrelation AR1 in both time series ($r = 0.31$; p-value <0.05; Fig. 5c). A non-significant relationship between the intensity of annual mean frequency of Puelche events and P95 HWs is found in the s1 subdomain during 1980–2020 (Fig. 5d). Despite this, the magnitude of Puelche events indicates an increasing trend of 0.2 m s^{-1} by decade. Significant relationships between the magnitude of Puelche events are observed along the 37°-40°S, however, some spatial differences are identified (Fig. 5e). The relationship between Tx CR2Met and the Puelche events in s2 indicates that high Tx values are associated with Puelche events with low magnitudes associated with easterly flow (Fig. 5f). We also found an increasing trend of Puelche events in s2, with an average rate of 0.74 events by decade (Fig. 5g). In addition, the relationship between yearly average of Puelche events and P95 HWs has recorded a significant relationship, particularly removing AR1 on the time series (Pearson r coefficient = 0.48; p-value <0.001). Conversely to

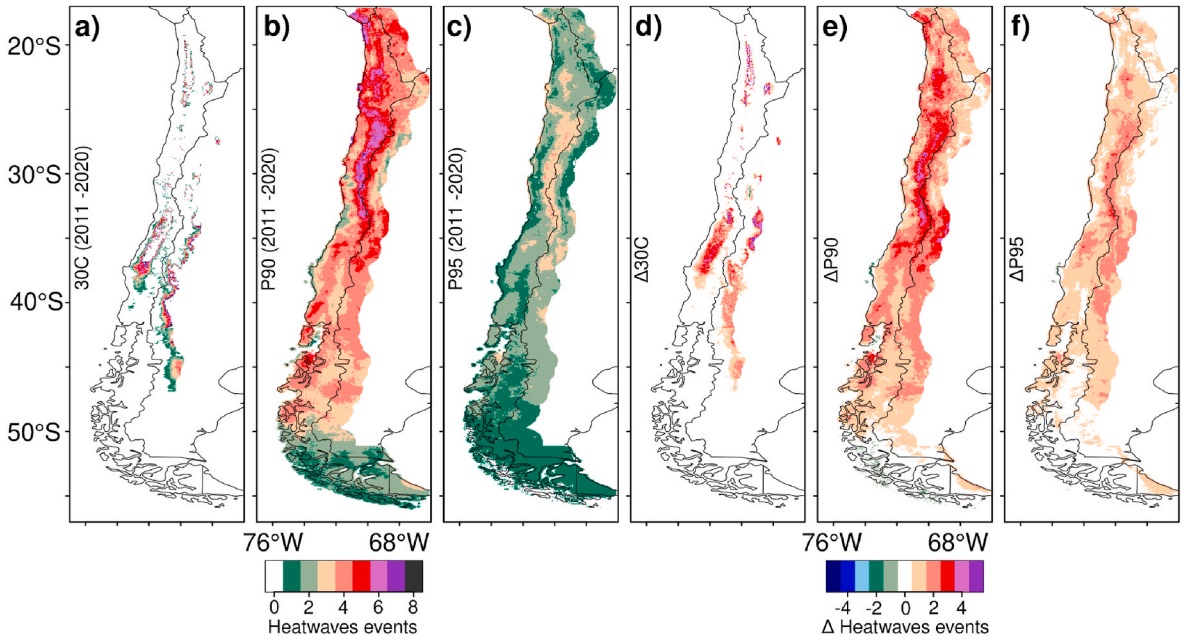

Fig. 4. Mean heatwave frequency during 2011–2020 based on the a) 30C, b) P90 and c) P95 thresholds. d-f) Heatwave frequency differences between 2011 - 2020 and 1980–2010 using the 30C, P90, and P95 thresholds, respectively.

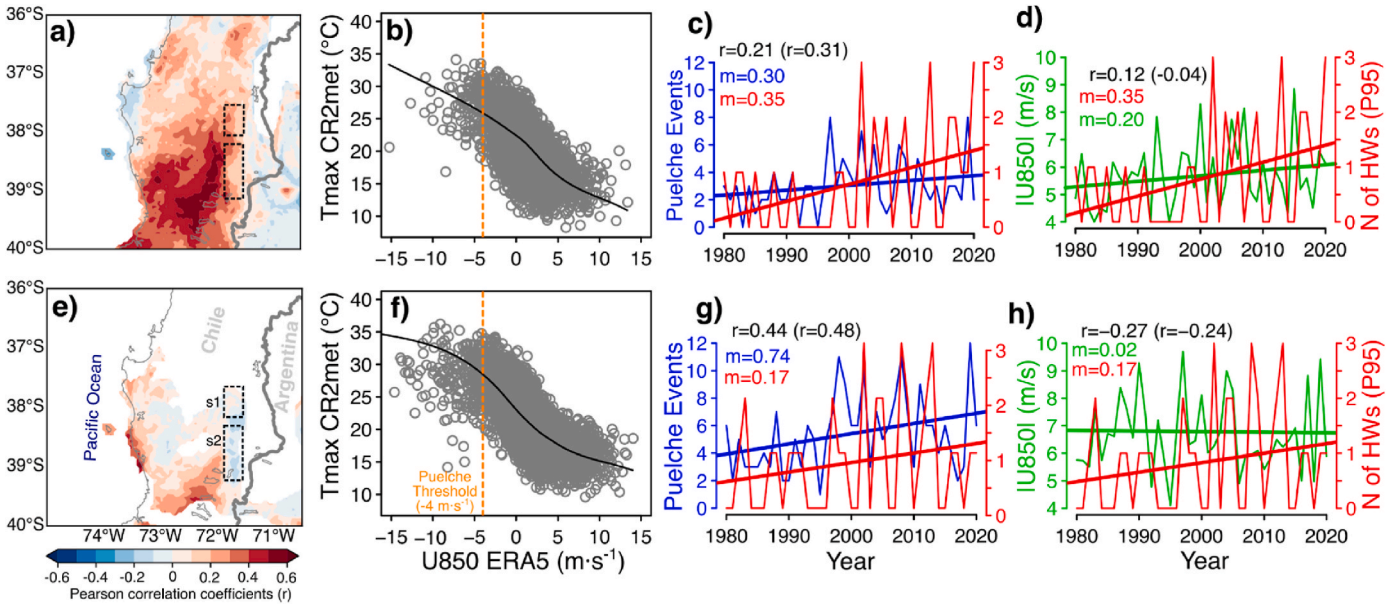

Fig. 5. a) Field of Pearson correlation coefficient between Puelche frequency (derived from ERA5 U850) and HWs (based on CR2Met Tx using the P95 threshold) for NDJFM 1980–2020 in the 36°-40°S region within South-Central Chile. Subdomains s1 and s2 were defined to analyze the relationship between the frequency of these HWs and the frequency and intensity of Puelche events, respectively. b) Scatterplot between the spatial averages of daily ERA5 U850 and CR2Met Tx for the s1 subdomain. The orange dashed line represents the U850 threshold of −4 m·s-1 used to define a Puelche event (see text). c) Time series of the seasonal number of Puelche events and the P95 HWs number within the s1 subdomain. d) Time series of the mean seasonal intensity of Puelche events and the P95 HWs number within the s1 subdomain; note that the absolute value of U850 is taken. e) Field of Pearson correlation coefficient between the intensity of Puelche events and P95 HW number. Panels f, g, and h are similar to panels b, c, and d, but for subdomain s2. The *r* values and values between parentheses in panels c, d, f, and g represent the Pearson correlation coefficient considering the first-order autocorrelation AR1 time series (without AR1). Significant Pearson *r* values at p-value <0.05 are those exceeding r = ± 0.30. On the same panels, *m* represents the slope, quantified as changes by decade of the respective variables. (For interpretation of the references to color in this figure legend, the reader is referred to the Web version of this article.)

recorded on s1 (Fig. 5d), the yearly average of P95 HWs in s2 exhibit a significant and negative relationship with the magnitude of Puelche events with and without removing the AR1 (values of −0.21 and −0.24, respectively; Fig. 5h). Our findings indicate that the Puelche frequency is one of the main local drivers of HWs episodes in South-Central Chile.

Indeed, high Tx days during NDJFM are associated with negative values of U850 at station 10 (TEM; Fig. 6a). We consider two subsamples of days with a clear distinction between their corresponding Tx distributions between 1980 and 2020. During non-Puelche events, the mean Tx at TEM reaches 22.9 °C (24.4 °C) using observations (CR2Met), whereas during Puelche events these values increase to 29.5 °C (29.9 °C), respectively (Fig. 6b). In addition, station data exhibit HWs

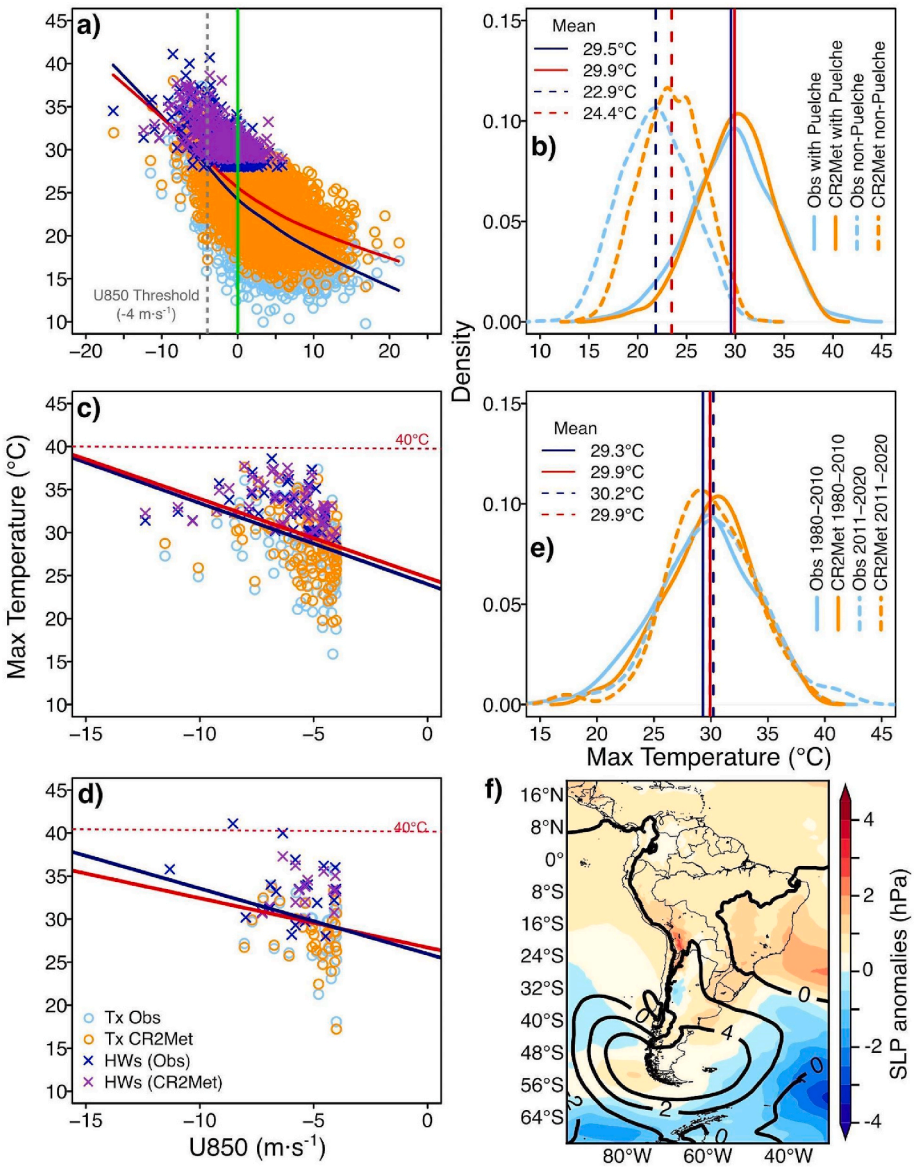

Fig. 6. a) Scatterplot between daily U850 from ERA5 (computed as a daily average from 00, 06, 12 and 18 UTC) and daily Tx at Temuco Station (TEM; number 10; light blue open circles) and CR2Met (orange open circles). The "x" symbol represents days classified as HWs using the corresponding P90 thresholds (blue for observations, violet for CR2Met). Continuous lines represent Locally Weighted Scatterplot Smoothing (Lowess) curves (blue for observations, red for CR2Met). The c) and d) panels are similar to a), but just for active Puelche days during 1980–2010 and 2011–2020 (the megadrought interval), respectively. As a reference, the horizontal red dashed line indicates 40 °C. b) Kernel density functions of Tx from observations (light blue) and CR2Met (orange) for days with active Puelche conditions (U850 < -4 m s^{-1}; continuous curves) and inactive non-Puelche conditions (dashed curves). e) As panel b, but for the superiods 1980–2010 and 2011–2020. f) Composite field of NDJFM SLP anomalies for Puelche days during 1980–2010 (black contour lines) and the difference computed by subtracting the Puelche composite for 2011–2020 minus the corresponding field from 1981 to 2010 (filled color contours). Anomalies are expressed in hPa units; source: ERA5. (For interpretation of the references to color in this figure legend, the reader is referred to the Web version of this article.)

episodes (after the P90 threshold) with Tx values exceeding 40 °C during the MD period, i.e., values that were not observed during the previous 1980–2010 period (Fig. 6c–d). We also identified a higher mean Tx for those days with Puelche activity during the MD period with respect to 1980–2010, with positive differences of 0.9 °C and equal Tx value using observations and CR2Met, respectively (Fig. 6e). We calculated the NDJFM SLP composite for Puelche days detected at TEM during 1981–2010 using ERA5 (Fig. 6f, black contours), and identify the synoptic pattern of a migratory anticyclone, which forces this wind system (Montecinos et al., 2017) and leads also to HWs in South-Central Chile (Jacques-Coper et al., 2021; Demortier et al., 2021). Next, we computed the difference field by subtracting the Puelche composite for 2011–2020 (MD period) minus the corresponding field from 1981 to 2010 (Fig. 6f, filled color contours). We observe a meridional dipole anomaly (of magnitude comparable to the 1981–2010 composite) that suggests a southward shift of the SLP anomaly center leading to Puelche days during the MD period. We hypothesize that this signal appears as a combination of the poleward shift of the stationary and migratory anticyclone signals, projected to continue towards the end of the 21st century (Aguirre et al., 2019). As stated by these authors, this process is consistent with an expansion of the Hadley cell, which is a manifestation of changes in the large-scale tropical atmospheric circulation under global warming (Lu et al., 2007). This phenomenon has been previously addressed for southern South America (Saurral et al., 2017).

All in all, Fig. 7 shows a scheme summarizing the main climate and synoptic forcings that modulate HWs frequency in Chile. As discussed in this study, anticyclonic regimes are the main driver of HWs. These can be conceptualized as a superposition of climate conditions (i.e., persistent features) –in particular, the position, intensity, and extension of the Southeastern Pacific Subtropical Anticyclone (SPSA, indicated in Fig. 8), which show an annual cycle and interannual and decadal variability–, and disturbances embedded in the synoptic variability range (i.e., transient features), specifically migratory anticyclones (the heart-shaped form in Fig. 6f and 7). As stated above, the poleward shift of stationary subtropical highs as the SPSA and transient migratory anticyclones are associated with the expansion of the Hadley cell within a warming world (Lu et al., 2007), which, in turn, is consistent with a poleward shift of the midlatitude Westerlies. This fact is a salient feature of climate change in the Southern Hemisphere (e.g., Thompson et al., 2011) and implies, among other impacts, a decrease in ventilation over western Patagonia during summer, thus increasing the seasonal Tx. We suggest that this warming mechanism might also tend to favor the

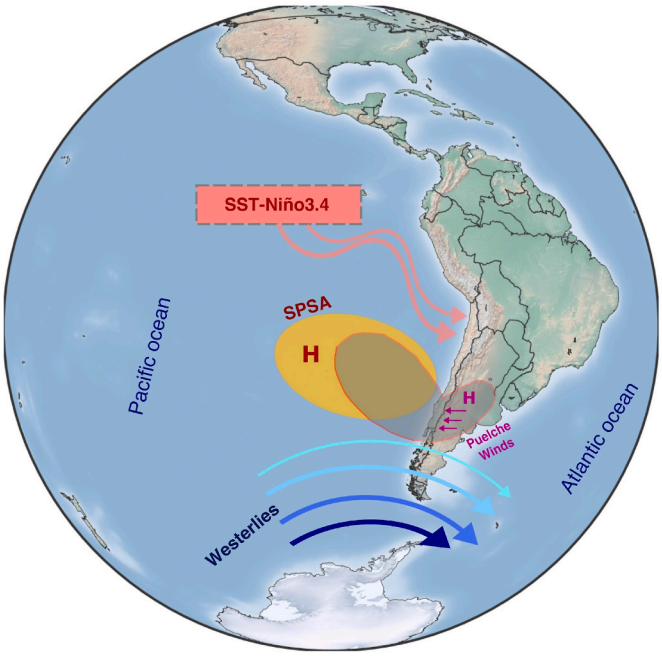

Fig. 7. Schematic overview of the main inter-annual climatic variability associated with heatwave trends across Chile: 1) Sea Surface Temperature (SST) within the El Niño 3.4 region in the tropical Pacific ocean (120°W-170°W; 5°N-5°S); 2) mean latitudinal position of the Southeastern Pacific Subtropical Anticyclone (SPSA), affecting, in turn, the latitudinal extent of the mid-latitude Westerlies and the frequency of migratory anticyclones, and 3) frequency and intensity of Puelche winds (Föhn-like easterly flow). Please refer to the main text for a description.

occurrence of HWs. Finally, both stationary and transient drivers of HWs are modulated by teleconnections stemming from climate variability modes, among which ENSO and SAM are particularly relevant for the study area considering the interannual timescale. In Fig. 8, teleconnections arising from ENSO SST anomalies (rooted in the equatorial Pacific, e.g. the Niño3.4 sector) are depicted by undulating vectors towards Chile. Additionally, it is worth commenting that coastal Tx is directly related to SST, so that ocean warming along the Peru-Chile coast is a main driver of HWs along the coastal zone, mainly in north and central Chile.

4. Discussion

Our results seem to be consistent with diverse studies devoted to HW trends in many other regions of the world that report upward frequency trends (Perkins et al., 2012; Russo et al., 2014; Piticar et al., 2018a; Zhang et al., 2017; Perkins-Kirkpatrick and Lewis 2020). We highlight the upward HW frequency trends observed along the Central Valley and Andes, from 30°S southward, where we identified an increasing HWs trend of 1 event per decade based on all thresholds (Fig. 3d–f). This region is of particular relevance for Chile, because of potential impacts, as more than 70% of the total population (INE 2017) concentrates between 30°S and 37°S and diverse main agro-economic activities are developed there, such as wine and fruit production, among others. In this section, we devote two subsections to discuss some specific aspects concerning temperature and HW trends and the possible role of the Megadrought (2010-onwards) in shaping the HW regime.

4.1. Temperature and HW frequency trends

We compared trends in Tx and HW frequency derived from CR2Met gridded data and station records using classic statistical metrics (R-squared, RMSE, and bias). Regarding Tx trends, Fig. S3 shows that these are more pronounced in instrumental records than CR2Met for stations located across the Central Valley and the Andes from ~33°S to the south (i.e., stations 6–18), with the exception of station 14 (FUT). In comparison with observation-derived trends, we found a positive (negative) bias in Tx trends based on CR2Met along the coastal Chilean area –namely stations ANT, LSE, VPO, CON, PMT, PAR– (slightly in STG and Patagonia, stations FUT, COY, CCH). In particular, CR2Met Tx is not able to reproduce the coastal Tx regime properly nor the multidecadal cooling trend along the Chilean coast reported by Falvey and Garreaud (2009). In fact, we observe such Tx cooling trends in instrumental records from stations 1–4, but not clearly in their corresponding CR2Met time series (Fig. S3). Nevertheless, according to Burger et al. (2018), this cooling trend has already finished in central Chile, a result that agrees with the observations in VPO but not with CR2Met (Fig. S3e).

Despite its suboptimal performance for Tx along the Central Valley and the coast, we observe that CR2Met satisfactorily reproduces the general HW regime. In other words, CR2Met performs well at identifying HW frequency and trend even in locations that exhibit moderate Tx validation metrics. In fact, HW frequency trends show an overall coherence between observations and CR2Met for 1980–2020 (Figs. S2d–f). Moreover, this is clear also when examining the seasonal behavior, shown for instance at station 8 (CHI) from November 2019 to March 2020 (Fig. 2). Indeed, regarding HW trends, we found acceptable R^2 values (0.4–0.45) in Southern Chile, mainly for locations south of station 9 (CON; Fig. 1c). Lower R^2 values (~0.3–0.35) were found in the north (stations 1 to 4, i.e. ARI to LSE) and central Chile, 7 (stations 7–8, CUR and CHI); hence, we warn to consider our results carefully for their respective surroundings.

HW frequency trends based on the 30C threshold reveal an increase in Northern Chile and across Central and South-Central Chile (Fig. 3d). In general terms, we observe upward HW trends across the Central Valley and over the Andes. These upward trends could be explained by the also upward Tx trends (Fig. S1), previously reported by Falvey and Garreaud (2009) and Burger et al. (2018). It is necessary to highlight some further discrepancies in HW frequency and trends calculated from observations and CR2Met. Along the coastal range in Northern Chile (stations 2 IQU and 3 ANT), HW frequency trends using the P90 and P95 thresholds exhibit nearly stationary values in CR2Met, whereas observation-based trends are clearly downward (Fig. 3e–f). Again, these discrepancies could be explained by the absence of a cooling signal in CR2Met Tx along the coast of North Chile (Fig. S3). In central Chile (stations 6–10; STG-TEM), HW frequency trends using the 30C threshold (Fig. 3d), are upward and steeper in observations than in CR2Met. Conversely, similar HW frequency trends are found for South-Central Chile and Patagonia using P90 and P95 from both datasets.

All in all, using CR2Met and the P90 and P95 thresholds, we identify an overall upward HWs trend in most of Chile (Fig. 3e–f). The prevailing upward HW frequency trends inferred from observations in our work are concordant with Piticar et al. (2018), despite the fact that this author used a different analysis period (1961–2016). Therefore, we computed Tx trends from observations for the longer period NDJFM 1962–2021 and confirmed that all records from station 5 to the south show upward trends. Indeed, the upward HW frequency trends are embedded within a warming trend for a major part of Chile. As an additional contribution, we show that the multidecadal evolution of intensity, a key parameter for HW, can be assessed by exploring trends in the highest Tx values for each NDJFM season (i.e., the hottest NDJFM day) and the 18 stations for the extended period 1961–2020. As shown in Fig. S4, we found overall upward trends, reaching values up to 0.5°C per decade at station 13 (PMT), with the exception being a slight downward trend of −0.04 °C per decade observed at station 9 (CON).

4.2. A possible relationship between HW trends, the megadrought and environmental implications

The increasing HWs frequency observed in Central Chile could

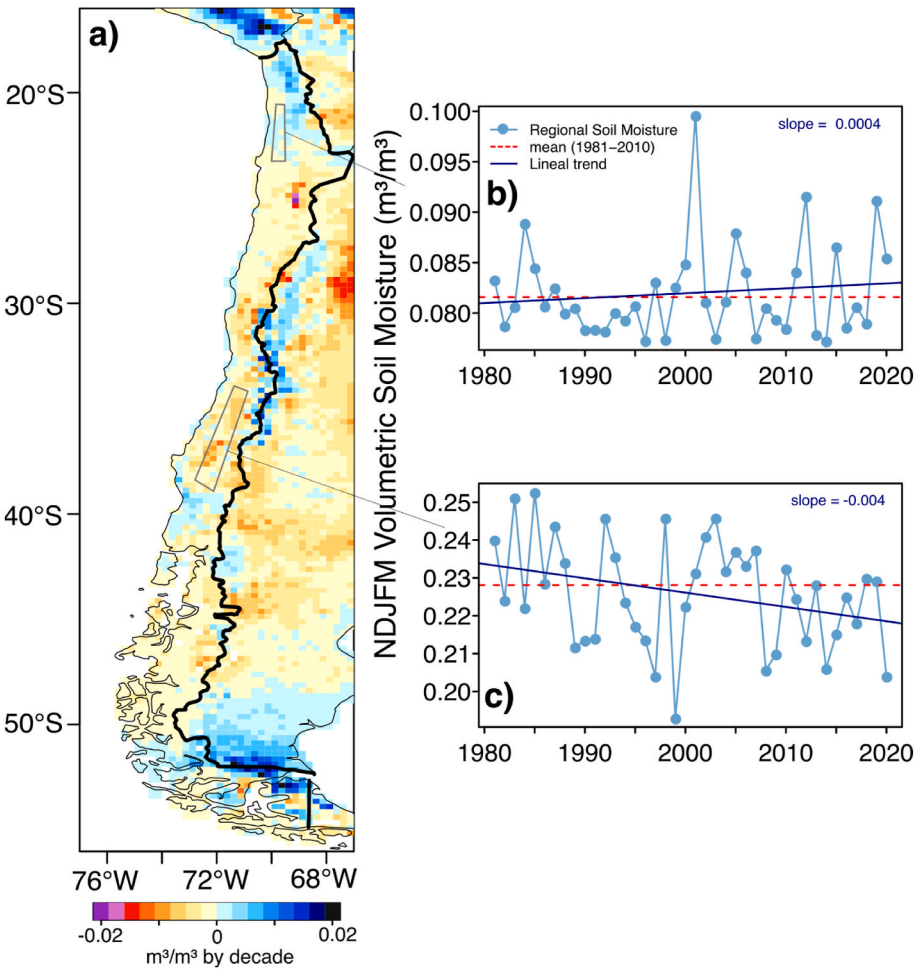

Fig. 8. Trends of November to March volumetric soil moisture at surface during 1981–2020 derived from GLEAM v3.5 product at ~25 km horizontal resolution. The b) and c) panels show the mean temporal variations of SM during 1981–2020 in both subregions considered as hotspots. The slope indicate in b and c panels represent m^3m^{-3} per decade.

potentially lead to severe ecosystemic perturbations on the Mediterranean forest, where one-third of the total area (~13,000 km^2) has shown a significant decrease in Normalized Difference Vegetation Index (NDVI; browning) during the recent MD period (Miranda et al., 2020). Additionally, tree-ring growth of native species from the Mediterranean forest, for instance, "Peumo" (*Cryptocarya alba*) and "Belloto del Norte" (*Beilschmiedia miersii*), exhibit a clear downward trend particularly during MD period (Venegas-González et al., 2022). Also, the upward HW frequency trends found from 33°S southward seem to be alarming given the cover of exotic forest plantations (e.g., *Pinus radiata, Eucalyptus globulus*) distributed between 33°-41°S (Aguayo et al., 2009; Vergara-Diaz et al., 2017), and the relationship between wildfires as is mentioned in González et al. (2011). In fact, the occurrence of an increasing number of HW over areas with large exotic forest plantations, in concomitance with long-term drought periods represents a high threat; for instance, Parente et al. (2018) indicate that 97% of the total number of extreme fires were active during HWs in Portugal between 1981 and 2010, in synchrony with more frequent drought episodes recorder on the Iberian Peninsula during the recent decades (Sousa et al., 2017). Recently, Ribeiro et al. (2020) found that preceding dry conditions based on the Standardized Precipitation Evaporation Index (SPEI) increase the probability of exceeding summer hot extremes in the Iberian Peninsula. Interestingly, these results seem to be valid for Chile, where our findings indicate increasing HW frequencies during 2011–2020 with respect to 1980–2010, using all thresholds (Fig. 4). Since 2010, Central and South-Central Chile have been experiencing a so-called megadrought (Garreaud et al., 2017). Hence, higher daily Tx might result in more intense and/or more persistent HWs, such as those events identified during 2017 that induce severe wildfires and impacts (more than 5 000 km^2 burned in Central Chile; Bowman et al., 2019). In fact, recent studies have addressed the role of droughts in amplifying characteristics of HWs (Miralles et al., 2014), especially in the case of Brazil (Geirinhas et al., 2021; Libonati et al., 2022), thus analyzing these phenomena from the perspective of compound events (Zscheisler et al., 2020). Focusing on the genesis of mega-heatwaves, a global study carried out by Miralles et al. (2014) highlighted the interaction of multiple factors, including synoptic patterns that lead to clear-sky conditions (such as the Puelche events between 38° and 40°S described above) and a reduction in soil moisture. We speculate that the persistent dry conditions registered in Chile since 2010 have played a key role in the increase in HW frequency during 2011–2020 in Chile reported here. In fact, dry soil conditions or less soil moisture provoke an amplification of air temperatures by the reduced latent cooling, producing local land-atmosphere feedback (Fischer et al., 2007). In order to explore this, we used surface soil moisture generated by the Global Land Amsterdam Model (GLEAM v3.5) at ~ 25 km of horizontal resolution (Martens et al., 2017). We identified a general downward trend of volumetric soil moisture at the surface (measured in m^3m^{-3}) in most of Chile during 1981–2020 (Fig. 8a). However, we observed an opposite trend between several HW hotspots identified, for instance, in Northern Chile. A slightly upward trend in soil moisture is recorded in the north HW hotspot (Fig. 8b), while the HW hotspot located in South-Central Chile

record an increasing linear trend during 1981–2020 (Fig. 8c). We think that soil moisture has a more important role in the frequency of HWs in south-central Chile compared to the north. As shown above, the South-Central Chile region shows an increasing HW trend using all thresholds, in particular, the Central Valley between 35°S and 39°S (Fig. 3d–f). To the South, Patagonian locations between 44° and 50°S also exhibit a downward trend in volumetric soil moisture. Particularly in these regions, we identified that HWs frequencies have increased by one to two more events during 2011–2020 with respect to 1980–2010 (Fig. 4e).

5. Conclusions

Heatwaves are a major threat to Chilean society. In this work, we examined HW frequency trends along Chile using NDJFM daily Tx derived from a gridded product produced by the Center of Climate and Resilience Research CR2 (CR2Met). This is the first study that uses this product to evaluate HWs in Chile, focusing on their spatiotemporal variations during 1980–2020. Our results include a statistical comparison between Tx extracted from CR2Met and 18 meteorological stations managed by the DMC, and the description of the spatial distribution and temporal evolution of NDJFM HW frequency based on a persistence criterion of three consecutive days with Tx over three intensity thresholds: (i) 30 °C, ii) Tx > 90th percentile (P90), and iii) Tx > 95th percentile (P95). We warn to consider our results carefully mainly in coastal locations across Chile, where we report discrepancies between Tx extracted from CR2Met and observations.

Considering all thresholds, HW frequency trends computed from observations and CR2Met are similar along the Central Valley (i.e., from ~30°S southward). However, discrepancies are evident in coastal areas (20°-25°S), where CR2Met overestimates observed Tx values. In this region, observed HW frequency trends were downward, but CR2Met exhibits upward Tx trends. Hence, our results are not reliable along coastal areas, especially in Northern Chile, because CR2Met does not capture the cooling trend observed during the last decades.

We found an overall upward trend in HW frequency during 1980–2020. Upward trends using the 30C threshold concentrate in Northern Chile (between ~20°-25°S) and in Central and South-Central Chile (between 33.5°S-39°S), with values of 1.5 HWs and ~0.75 to 1.25 HWs events per decade, respectively. Trends based on the P90 threshold exhibit upward patterns in most of Chile, including the Andes in Northern Chile (18°-34°S), the Central Valley (between 33° - 41°S), North Patagonia, and Tierra del Fuego. In most of these subregions, HW frequency trends are around 1 event per decade. HWs based on the P95 threshold exhibit upward trends between 18° - 50°S, mostly concentrated over the Andes from Northern Chile (18°S - 34°S), and along the Central Valley and the Andes from 35°S - 42°S, with values between 0.25 and 0.75 events per decade at these latitudes.

The megadrought period during 2011–2020 exhibits overall upward changes in mean HWs frequency with respect to 1980–2010. Based on the P90 threshold, we observe between 2 and 4 more HWs per season than during the previous interval from North to Central Chile (~20°-35°S), mostly concentrated along the Andes. High upward HW frequency changes present a cluster between 29° and 34°S over the Andes. Further upward changes (+1–3 HWs) were identified along the Central Valley between 35° and 43°S, including the Chiloe island. Lower increases (+1–2 HWs) were found over Patagonia. HWs events based on the P95 threshold also exhibit upward changes during 2011–2020 with respect to 1980–2010 around ~23°S and between 25° and 35°S in the Andes (+2–3 HWs), around ~35°S in the Central Valley (+1–3 HWs), and from 35° southward (+1–3 HWs). Meanwhile, no changes were recorded in Patagonia and several coastal locations in Chile around 30°, 33°, and 37°S. The drought-HW-wildfire feedback seems to be also relevant if we consider that the anthropogenic contribution to the current megadrought in Chile is estimated as ~25% (Boisier et al., 2016), and Central Chile has shown an increased risk of drought since 1950 onwards, as inferred from instrumental measurements of streamflow and precipitation (González-Reyes et al., 2017).

HWs in central and Southern Chile occur during anticyclonic conditions (Jacques-Coper et al., 2021; Demortier et al., 2021). These weather patterns might be understood as resulting from the superposition of climate conditions (i.e., persistent features) –in particular, the position, intensity and extension of the SPSA– and transient perturbations. Both factors might be, in turn, modulated by internal climate modes and externally forced climate change. In this sense, the southward SPSA migration and a southward-shifted track of migratory anticyclones are two possible consequences of the expansion of the Hadley cell within a warming world (Lu et al., 2007). We speculate that these factors might explain in part the trends found for HW frequency in Southern Chile (Fig. 8). Moreover, anticyclonic regimes induce easterly, Foehn-like winds called Puelche in Southern Chile (Montecinos et al., 2017). Puelche events favor a cloudless sky and a drier atmosphere, two conditions that eventually promote the occurrence of HWs. Indeed, we found a subtle seasonal relationship between the frequency of Puelche events and the frequency of P95 HWs over Southern Chile towards the Andes, around 39°S (Fig. 5).

The results reported here highlight the need for increased efforts to deepen the research on climate extreme events in Chile and focusing on their spatial and temporal signatures. Also, future efforts should aim at understanding feedback between extreme events such as drought and heatwaves, considering future climate projections for Chile that indicate severe precipitation reductions and an upward trend in air temperature, in particular over the Andes.

Our approach to assessing the HW trends and possible local drivers presented here is a contribution to the understanding of HWs evolution in this part of the world, considering the lack of this kind of research in South America (Hartmann et al., 2013; Rusticucci et al., 2016). Future studies should focus on untangling the feedback between HWs, soil moisture, and drought, as well as on describing temporal relationships between HWs and global-scale climatic forcings such as ENSO and SAM. All these points are highly relevant to better understanding current and future climate change scenarios in Chile.

Credit author statement

A. González-Reyes: Conceptualization, Methodology, Formal analysis, Programming, Visualization, Writing- original draft preparation.

M. Jacques-Coper: Conceptualization, Methodology, Formal analysis, Visualization, Writing- original draft preparation.

C. Bravo: Methodology, Visualization, Writing- original draft preparation.

Maisa Rojas: Writing- original draft preparation.

R. Garreaud: Writing- original draft preparation.

Declaration of competing interest

The authors declare that they have no known competing financial interests or personal relationships that could have appeared to influence the work reported in this paper.

Data availability

Data will be made available on request.

Acknowledgments

The authors thank Juan Pablo Boisier for CR2Met v2.0, the National Weather Directorate of Chile (DMC) for the availability of meteorological records, and the Chilean National Agency for Research and Development (ANID) for partial funding through the Center for Climate and Resilience Research (CR2, ANID/FONDAP/15110009, ANID/FONDAP/1522A0001). A. González-Reyes thanks grant ANID/PAI/77190101,

ANID/FONDECYT/1201411, ANID/FONDECYT/11230437 and ANID/SEQUIA/FSEQ210022 projects. MJC also thanks grants ANID/FONDECYT/11170486 and ANID/PAI/79160105.

Appendix A. Supplementary data

Supplementary data to this article can be found online at https://doi.org/10.1016/j.wace.2023.100588.

References

Aguayo, M., Pauchard, A., Azócar, G., Parra, O., 2009. Cambio del uso del suelo en el centro sur de Chile a fines del siglo XX: entendiendo la dinámica espacial y temporal del paisaje. Rev. Chil. Hist. Nat. 82 (3), 361–374. https://doi.org/10.4067/S0716-078X2009000300004.

Aguirre, C., Rojas, M., Garreaud, R.D., Rahn, D., 2019. Role of synoptic activity on projected changes in upwelling-favourable winds at the ocean's eastern boundaries. npj Clim. Atmos. Sci. 2, 44. https://doi.org/10.1038/s41612-019-0101-9.

Aguirre, F., Squeo, F.A., López, D., Grego, R.D., Buma, B., Carvajal, D., Jaña, R., Casassa, G., Rozzi, R., 2021. Gradientes Climáticos y su alta influencia en los ecosistemas terrestres de la Reserva de la Biosfera Cabo de Hornos, Chile, vol. 49. Anales Del Instituto De La Patagonia. https://doi.org/10.22352/AIP202149012.

Alvarez-Garreton, C., Mendoza, P.A., Boisier, J.P., Addor, N., Galleguillos, M., Zambrano-Bigiarini, M., Lara, A., Puelma, C., Cortes, G., Garreaud, R., McPhee, J., Ayala, A., 2018. The CAMELS-CL dataset: catchment attributes and meteorology for large sample studies – Chile dataset, Hydrol. Earth Syst. Sci. 22, 5817–5846. https://doi.org/10.5194/hess-22-5817-2018.

Ancapichún, S., Garcés-Vargas, J., 2015. Variability of the Southeast Pacific Subtropical Anticyclone and its impact on sea surface temperature off north-central Chile. Cienc. Mar. 41 (1), 1–20. https://doi.org/10.7773/cm.v41i1.2338.

Ayala, Á., Farías-Barahona, D., Huss, M., Pellicciotti, F., McPhee, J., Farinotti, D., 2020. Glacier runoff variations since 1955 in the Maipo River basin, in the semiarid Andes of central Chile. Cryosphere 14, 2005–2027. https://doi.org/10.5194/tc-14-2005-2020.

Boisier, J.P., Rondanelli, R., Garreaud, R.D., Muñoz, F., 2016. Anthropogenic and natural contributions to the Southeast Pacific precipitation decline and recent megadrought in central Chile. Geophys. Res. Lett. 43, 413–421. https://doi.org/10.1002/2015GL067265.

Boisier, J.P., Alvarez-Garretón, C., Cordero, R.R., Damiani, A., Gallardo, L., Garreaud, R. D., Lambert, F., Ramallo, C., Rojas, M., Rondanelli, R., 2018. Anthropogenic drying in central-southern Chile evidenced by long-term observations and climate model simulations. Elem Sci. Anth. 6 (1) https://doi.org/10.1525/elementa.328.

Boisier, J.P., 2023. CR2MET: a high-resolution precipitation and temperature dataset for the period 1960-2021 in continental Chile. Zenodo. https://doi.org/10.5281/zenodo.7529682 (v2.5) [Data set].

Bowman, D., Williamson, G., Abatzoglou, J., Kolden, C.A., Cochrane, M.A., Smith, A.M., 2017. Human exposure and sensitivity to globally extreme wildfire events. Nat. Ecol. Evol. 1, 0058 https://doi.org/10.1038/s41559-016-0058.

Bowman, D.M., Moreira-Munoz, A., Kolden, C.A., Chavez, R.O., Muñoz, A.A., Salinas, F., González-Reyes, A., Rocco, R., De la Barrera, F., Williamson, G.J., Borchers, N., 2019. Human-environmental drivers and impacts of the globally extreme 2017 Chilean fires. Ambio 48 (4), 350–362. https://doi.org/10.1007/s13280-018-1084-1, 2019.

Bozkurt, D., Rojas, M., Boisier, J.P., et al., 2019. Dynamical downscaling over the complex terrain of southwest South America: present climate conditions and added value analysis. Clim. Dynam. 53, 6745–6767. https://doi.org/10.1007/s00382-019-04959-y.

Bravo, C., Loriaux, T., Rivera, A., Brock, B.W., 2017. Assessing glacier melt contribution to streamflow at Universidad Glacier, central Andes of Chile. Hydrol. Earth Syst. Sci. 21, 3249–3266. https://doi.org/10.5194/hess-21-3249-2017.

Burger, F., Brock, B., Montecinos, A., 2018. Seasonal and elevational contrasts in temperature trends in Central Chile between 1979 and 2015. Global Planet. Change 162, 136–147. https://doi.org/10.1016/j.gloplacha.2018.01.005.

Ceccherini, G., Russo, S., Ameztoy, I., Romero, C.P., Carmona-Moreno, C., 2016. Magnitude and frequency of heat and cold waves in recent decades: the case of South America. Nat. Hazards Earth Syst. Sci. 16, 821–831. https://doi.org/10.5194/nhess-16-821-2016.

De la Barrera, F., Barraza, F., Favier, P., Ruiz, V., Quense, J., 2018. Megafires in Chile 2017: monitoring multiscale environmental impacts of burned ecosystems. Sci. Total Environ. 637, 1526–1536. https://doi.org/10.1016/j.scitotenv.2018.05.119.

Demortier, A., Bozkurt, D., Jacques-Coper, M., 2021. Identifying key driving mechanisms of heat waves in central Chile. Clim. Dynam. 57, 2415–2432. https://doi.org/10.1007/s00382-021-05810-z.

Donat, M.G., Alexander, L.V., Yang, H., et al., 2013. Updated analyses of temperature and precipitation extreme indices since the beginning of the twentieth century: the HadEX2 dataset. J. Geophys. Res. 118, 2098–2118. https://doi.org/10.1002/jgrd.50150.

Falvey, M., Garreaud, R.D., 2009. Regional cooling in a warming world: recent temperature trends in the southeast Pacific and along the west coast of subtropical South America (1979–2006). J. Geophys. Res. 114, D04102 https://doi.org/10.1029/2008JD010519.

Feron, S., Cordero, R.R., Damiani, A., Llanillo, P.J., Jorquera, J., Sepulveda, E., Asencio, V., Laroze, F., Labbe, J., Carrasco, J., Torres, G., 2019. Observations and projections of heat waves in South America. Sci. Rep. 9, 8173. https://doi.org/10.1038/s41598-019-44614-4.

Fischer, E.M., Seneviratne, S.I., Lüthi, D., Schär, C., 2007. Contribution of land–atmosphere coupling to recent European summer heat waves. Geophys. Res. Lett. 34, L06707 https://doi.org/10.1029/2006GL029068.

Garreaud, R., Vuille, M., Compagnucci, R., Marengo, J., 2009. Present day South American climate. Palaeogeogr. Palaeoclimatol. Palaeoecol. 281, 180–195. https://doi.org/10.1016/j.palaeo.2007.10.032.

Garreaud, R.D., Alvarez-Garreton, C., Barichivich, J., Boisier, J.P., Christie, D., Galleguillos, M., LeQuesne, C., McPhee, J., Zambrano-Bigiarini, M., 2017. The 2010–2015 megadrought in central Chile: impacts on regional hydroclimate and vegetation. Hydrol. Earth Syst. Sci. 21, 6307–6327. https://doi.org/10.5194/hess-21-6307-2017.

Geirinhas, J.L., Russo, A., Libonati, R., Sousa, P.M., Miralles, D.G., Trigo, R.M., 2021. Recent increasing frequency of compound summer drought and heatwaves in Southeast Brazil. Environ. Res. Lett. 16 (3), 034036.

González, M., Lara, A., Urrutia, R., Bosnich, J., 2011. Cambio climático y su impacto potential en la ocurrencia de incendios forestales en la zona centro-sur de Chile (33° - 42° S). Bosque (Valdivia) 32 (3), 215–219. https://doi.org/10.4067/S0717-92002011000300002.

González-Reyes, Á., 2016. Ocurrencia de eventos de sequías en la ciudad de Santiago de Chile desde mediados del siglo XIX. Rev. Geogr. Norte Gd. (64), 21–32. https://doi.org/10.4067/S0718-34022016000200003.

González-Reyes, Á., McPhee, J., Christie, D.A., Le Quesne, C., Szejner, P., Masiokas, M. H., Villalba, R., Muñoz, A.A., Crespo, S., 2017. Spatiotemporal variations in hydroclimate across the Mediterranean Andes (30°–37°S) since the early twentieth century. J. Hydrometeorol. 18 (7), 1929–1942. https://doi.org/10.1175/JHM-D-16-0004.1.

Hartmann, D.L., Klein Tank, A.M.G., Rusticucci, M., Alexander, L.V., Bronnimann, S., Charabi, Y., Dentener, F.J., Dlugokencky, E.J., Easterling, D.R., Kaplan, A., Soden, B. J., Thorne, P.W., Wild, M., Zhai, P.M., 2013. Observations: atmosphere and surface, 2013. In: Stocker, T.F., Qin, D., Plattner, G.-K., Tignor, M., Allen, S.K., Boschung, J., Nauels, A., Xia, Y., Bex, V., Midgley, P.M. (Eds.), Climate Change 2013: the Physical Science Basis. Contribution of Working Group I to the Fifth Assessment Report of the Intergovernmental Panel on Climate Change. Cambridge University Press, Cambridge, United Kingdom and New York, NY, USA. Observations: atmosphere and surface.

Hersbach, H., Bell, B., Berrisford, P., Hirahara, S., Horányi, A., Mũnoz-Sabater, J., Nicolas, J., Peubey, C., Radu, R., Schepers, D., Simmons, A., Soci, C., Abdalla, S., Abellan, X., Balsamo, G., Bechtold, P., Biavati, G., Bidlot, J., Bonavita, M., De Chiara, G., Dahlgren, P., Dee, D., Diamantakis, M., Dragani, R., Flemming, J., Forbes, R., Fuentes, M., Geer, A., Haimberger, L., Healy, S., Hogan, R.J., Hólm, E., Janisková, M., Keeley, S., Laloyaux, P., Lopez, P., Lupu, C., Radnoti, G., de Rosnay, P., Rozum, I., Vamborg, F., Villaume, S., Thépaut, J.-N., 2020. The ERA5 global reanalysis Q. J. R. Meteor. Soc. 146, 1999–2049. https://doi.org/10.1002/qj.3803.

Holz, A., Paritsis, J., Mundo, I.A., Veblen, T.T., Kitzberger, T., Williamson, G.J., Aráoz, E., Bustos-Schindler, C., González, M., Grau, H.R., Quezada, J.M., 2017. Southern Annular Mode drives multicentury wildfire activity in southern South America. Proc. Natl. Acad. Sci. USA 114, 9552–9557. https://doi.org/10.1073/pnas.1705168114.

Instituto Nacional de Estadisticas INE., 2017. Chile census. http://www.censo2017.cl/.

Intergovermental Panel on Climate Change (IPCC), 2021. The Physical Science Basis. Technical Summary. Cambridge University Press, Cambridge, United Kingdom and New York, NY, USA. https://doi.org/10.1017/9781009157896 (in press).

Jacques-Coper, M., Veloso-Aguila, D., Segura, Ch, Valencia, A., 2021. Intraseasonal teleconnections leading to heat waves in Central Chile. Int. J. Climatol. 41, 4712–4731. https://doi.org/10.1002/joc.7096.

Kjellstrom, T., 2016. Impact of climate conditions on occupational health and related economic losses: a new feature of global and urban health in the context of climate change. Asia Pac. J. Publ. Health 28 (2_Suppl. l), 28S–37S. https://doi.org/10.1177/1010539514568711.

Libonati, R., Geirinhas, J.L., Silva, P.S., Russo, A., Rodrigues, J.A., Belem, L.B.C., Nogueira, J., Roque, F.O., DaCamara, C.C., Nunes, A.M.B., Marengo, J.A., Trigo, R. M., 2022. Assessing the role of compound drought and heatwave events on unprecedented 2020 wildfires in the Pantanal. Environ. Res. Lett. 17 (1), 015005.

Lu, J., Vecchi, G.A., Reichler, T., 2007. Expansion of the Hadley cell under global warming. Geophys. Res. Lett. 34 https://doi.org/10.1029/2006gl028443.

Martens, B., Miralles, D.G., Lievens, H., Van der Schalie, R., de Jeu, R.A.M., Fernández-Prieto, D., Beck, H.E., Dorigo, W.A., Verhoest, N.E.C., 2017. GLEAM v3: satellite-based land evaporation and root-zone soil moisture. Geosci. Model Dev. (GMD) 10, 1903. https://doi.org/10.5194/gmd-10-1903-2017. –1925.

Martínez-Retureta, R., Aguayo, M., Abreu, N.J., Stehr, A., Duran-Llacer, I., Rodríguez-López, L., Sauvage, S., et al., 2021. Estimation of the climate change impact on the hydrological balance in basins of south-Central Chile. Water 13 (6), 794. https://doi.org/10.3390/w13060794. MDPI AG.

McMichael, A.J., Lindgren, E., 2011. Climate change: present and future risks to health, and necessary responses. J. Intern. Med. 270, 401–413. https://doi.org/10.1111/j.1365-2796.2011.02415.x.

Miralles, D.G., Teuling, A.J., van Heerwaarden, C.C., Vilà-Guerau de Arellano, J., 2014. Mega-heatwave temperatures due to combined soil desiccation and atmospheric heat accumulation. Nat. Geosci. 7, 345–349. https://doi.org/10.1038/ngeo2141.

Miranda, A., Lara, A., Altamirano, A., Di Bella, C., González, M.E., Camarero, J.J., 2020. Forest browning trends in response to drought in a highly threatened mediterranean landscape of South America. Ecol. Indicat. 115, 106401 https://doi.org/10.1016/j.ecolind.2020.106401.

Montecinos, A., Muñoz, R.C., Oviedo, S., Martínez, A., Villagrán, V., 2017. Climatological characterization of Puelche winds down the western slope of the extratropical Andes mountains using the NCEP climate forecast system reanalysis. J. Appl. Meteorol. Climatol. 56 (3), 677–696. https://doi.org/10.1175/JAMC-D-16-0289.1.

Muñoz, A.A., Klock-Barría, K., Alvarez-Garreton, C., Aguilera-Betti, I., González-Reyes, Á., Lastra, J.A., Chávez, R.O., Barría, P., Christie, D., Rojas-Badilla, M., LeQuesne, C., 2020. Water crisis in petorca basin, Chile: the combined effects of a mega-drought and water management. Water 12 (3), 648. https://doi.org/10.3390/w12030648.

Parente, J., Pereira, M.G., Amraoui, M., Fischer, E.M., 2018. Heat waves in Portugal: current regime, changes in future climate and impacts on extreme wildfires. Sci. Total Environ. 631, 534–549. https://doi.org/10.1016/j.scitotenv.2018.03.044.

Pelto, M.S., Dryak, M., Pelto, J., Matthews, T., Perry, L.B., 2022. Contribution of glacier runoff during heat waves in the Nooksack river basin USA. Water 14, 1145. https://doi.org/10.3390/w14071145.

Perkins, S.E., Alexander, L.V., Nairn, J.R., 2012. Increasing frequency, intensity and duration of observed global heatwaves and warm spells. J. Geophys. Res. Letters 39, L20714. https://doi.org/10.1029/2012GL053361.

Perkins, S.E., 2015. A review on the scientific understanding of heatwaves-Their measurement, driving mechanisms, and changes at the global scale. Atmos. Res. https://doi.org/10.1016/j.atmosres.2015.05.014.

Perkins-Kirkpatrick, S.E., Lewis, S.C., 2020. Increasing trends in regional heatwaves. Nat. Commun. 11, 3357. https://doi.org/10.1038/s41467-020-16970-7.

Piticar, A., Croitoru, A.E., Ciupertea, F.-A., Harpa, G.V., 2018. Recent changes in heat waves and cold waves detected based on excess heat factor and excess cold factor in Romania. Int. J. Climatol. 38, 1777–1793. https://doi.org/10.1002/joc.5295.

Piticar, A., 2018. Changes in heat waves in Chile. Global Planet. Change 169, 234–246.

Ponce, R., Blanco, M., Giupponi, C., 2014. The economic impacts of climate change on the Chilean agricultural sector: a non-linear agricultural supply model. Chil. J. Agric. Res. 74 (4), 404–412. https://doi.org/10.4067/S0718-58392014000400005.

Quintana, J.M., Aceituno, P., 2012. Changes in the rainfall regime along the extratropical west coast of South America (Chile): 30°–43°S. Atmósfera 25, 1–22.

R Core Team, 2020. R: A Language and Environment for Statistical Computing. R Foundation for Statistical Computing, Vienna, Austria. URL. https://www.R-project.org/.

Ribeiro, A.F.S., Russo, A., Gouveia, CéM., Pires, C.A.L., 2020. Drought-related hot summers: a joint probability analysis in the Iberian Peninsula. Weather Clim. Extrem. 30, 100279 https://doi.org/10.1016/j.wace.2020.100279.

Rusticucci, M., Kyselý, J., Almeira, G., Lhotka, O., 2016. Long-term variability of heat waves in Argentina and recurrence probability of the severe 2008 heat wave in Buenos Aires. Theor. Appl. Climatol. 124, 679–689. https://doi.org/10.1007/s00704-015-1445-7.

Russo, S., Dosio, A., Graversen, R.G., Sillmann, J., Carrao, H., Dunbar, M.B., Singleton, A., Montagna, P., Barbola, P., Vogt, J.V., 2014. Magnitude of extreme heat waves in present climate and their projection in a warming world. J. Geophys. Res. Atmos. 119 (12), 512. https://doi.org/10.1002/2014JD022098, 500– 12.

Rutllant, J., Fuenzalida, H., 1991. Synoptic aspects of the central Chile rainfall variability associated with the Southern Oscillation. Int. J. Climatol. 11, 63–76.

Sarricolea, P., Herrera-Ossandon, M., Meseguer-Ruiz, O., 2017. Climatic regionalisation of continental Chile. J. Maps 13 (2), 66–73. https://doi.org/10.1080/17445647.2016.1259592.

Saurral, R.I., Camilloni, I.A., Barros, V.R., 2017. Low-frequency variability and trends in centennial precipitation stations in southern South America. Int. J. Climatol. 37, 1774–1793. https://doi.org/10.1002/joc.4810.

Sousa, P.M., Trigo, R.M., Barriopedro, D., Soares, P.M., Santos, J.A., 2017. European temperature responses to blocking and ridge regional patterns. Clim. Dynam. 1–21.

Thompson, D., Solomon, S., Kushner, P., et al., 2011. Signatures of the Antarctic ozone hole in Southern Hemisphere surface climate change. Nat. Geosci. 4, 741–749. https://doi.org/10.1038/ngeo1296.

Thornton, P.K., van de Steeg, J., Notenbaert, A., Herrero, M., 2009. The impacts of climate change on livestock and livestock systems in developing countries: a review of what we know and what we need to know. Agric. Syst. 101, 113–127.

Urrutia-Jalabert, R., González, M., González-Reyes, M., Lara, A., Garreaud, R., 2018. Climate variability and forest fires in central and south-central Chile. Ecosphere 9, e02171. https://doi.org/10.1002/ecs2.2171.

Venegas-González, A., Muñoz, A.A., Carpintero-Gibson, S., González-Reyes, Á., Schneider, I., Gipolou-Zuñiga, T., Aguilera-Betti, I., Roig, F., 2022. Sclerophyllous forest tree growth under the influence of a historic megadrought in the mediterranean ecoregion of Chile. Ecosystems. https://doi.org/10.1007/s10021-022-00760-x.

Vergara-Diaz, G., Sandoval-Vasquez, V., Herrera-Machuca, M., 2017. Spatial distribution of forest plantations in southern Chile, an area with a pulp mill. Revista Chapingo serie ciencias forestales y del ambiente 23 (1), 121–135. https://doi.org/10.5154/r.rchscfa.2015.09.045. ISSN 2007-4018.

Zhang, R., Chen, Z.-Y., Ou, C.-Q., Zhuang, Y., 2017. Trends of heat waves and cold spells over 1951–2015 in Guangzhou. China. Atmosphere. https://doi.org/10.3390/atmos8020037.

Zscheischler, J., Martius, O., Westra, S., et al., 2020. A typology of compound weather and climate events. Nat. Rev. Earth Environ. 1, 333–347. https://doi.org/10.1038/s43017-020-0060-z.